



OPEN

DATA DESCRIPTOR

High frequency Lunar Penetrating Radar quality control, editing and processing of Chang'E-4 lunar mission

G. Roncoroni¹✉, E. Forte¹, I. Santin¹, A. Černok¹, A. Rajšić², A. Frigeri³ & M. Pipan¹

Chinese lunar landing mission Chang'E-4 reached the far side of the Moon in January 2019 and has been providing unprecedented Lunar Penetrating Radar data able to explore the lunar subsurface down to more than 40 m (with its more resolute high frequency band). Data are periodically released to the scientific community in raw PDS4 format. Here we provide different versions of the radar dataset after editing (i.e. pre-processing), partial, and full processing in order to provide a complete ready-to-use dataset to end-users (data collected since 4th January 2019 until 27th March 2023) which can be directly exploited for analysis, interpretation, inversion, as well as integration with imagery or other information. In particular, we implemented an efficient and objective way to remove duplicated traces representing more than 90% of original data, as well as a processing flow able to retain all the original data information, while avoiding redundancies. The provided datasets can be implemented with future data releases and straightforwardly exploited for any future analysis.

Background & Summary

The Chinese lunar landing mission Chang'E-4 (CE-4) landed on January 3rd, 2019, in the ancient Van Kármán crater (diameter $D = 185$ km; 177.5991°E , 45.4446°S), located on the far side of the Moon¹. CE-4 mission follows the previous CE-3 mission, which aimed at the exploration of the lunar subsurface structures through a Lunar Penetrating Radar (LPR) while analysing the mineralogical composition by collecting *in situ* reflectance spectra and taking panoramic photographs. To achieve this, the Yutu-2 rover², of the CE-4 mission, is equipped with a dual frequency LPR, with central frequencies equal to 60 and 500 MHz (respectively CH-1 and CH-2), among several other sensors. LPR instruments is almost identical to Ground Penetrating Radar (GPR) devices commonly adopted as a near surface high-resolution geophysical tool on the Earth's surface. The low-frequency data of the LPR system are affected by interference phenomena first described for the CE-3 mission³ and then reported also for that of the CE-4⁴. Our work focuses on the high-frequency LPR dataset because of its high quality and potential information content emerged from several preliminary analyses e.g.^{2,5}.

The fundamental goal of the LPR survey is to investigate the lunar subsurface along the rover's path down to several tens or even hundreds of meters^{6–8}, with horizontal and vertical spatial resolutions of ~ 0.1 meter. Since landing, the rover has been moving along an irregular path, segmented into sectors separated by many stops and turnaround points. The initial studies focused on the first hundreds of meters of the path by applying different analysis, processing, and inversion algorithms^{8,9}, with the main aim of improving data interpretation^{6–10}. LPR data are publicly released through moon.bao.ac.cn/ website with a delay to the acquisition, due to an embargo period. Up to now (July 2023) a total of 634,419 A-scans (i.e. traces) for a total length of the path equal to ~ 1440 m, within the SOL range (i.e. each single data file identification number) between 01 (4th January 2019) and 286 (27th March 2023) for a total of 160 SOL files, have been released.

Our methodology aims at providing a standard workflow to get PDS4 and SEG-Y (IBM float 4 bytes) edited and processed LPR data ready for the interpretation process, starting from the original dataset release in separated PDS4 format files (Fig. 1). While PDS4 is a format used primarily by NASA to store and distribute solar,

¹Department of Mathematics, Informatics and Geosciences, University of Trieste, Trieste, Italy. ²Department of Earth, Atmospheric and Planetary Sciences, Purdue University, West Lafayette, Indiana, USA. ³Istituto di Astrofisica e Planetologia Spaziali (IAPS), Istituto Nazionale di Astrofisica (INAF), Rome, Italy. ✉e-mail: groncoroni@units.it

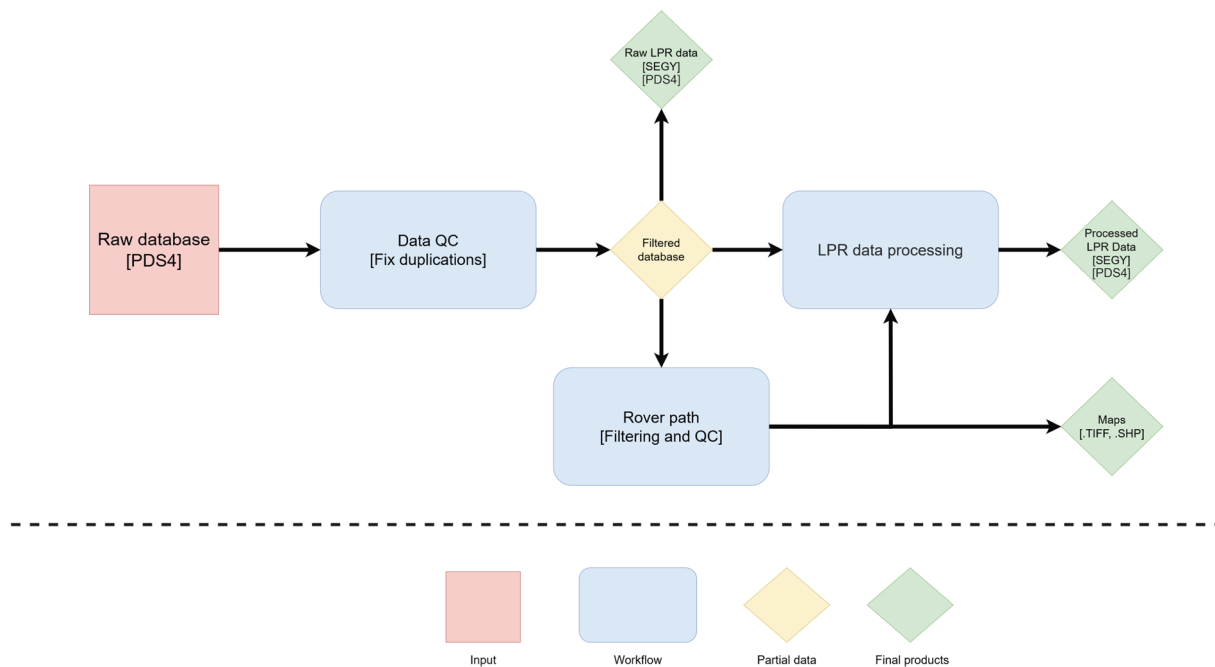


Fig. 1 PDS4 database (input), in red; workflow of the methodology, in blue; available dataset from the current work (outputs), in green. QC refers to the quality control steps applied to the data.

lunar and planetary imagery data (<https://pds.nasa.gov/datastandards/documents/>), SEG-Y is the standard format developed by the Society of Exploration Geophysicists (SEG) to store reflection seismic geophysical data¹¹ (<http://seg.org/Publications/SEG-Technical-Standards>). Raw database files contain both spatial information (e.g. rover path coordinates) and the raw LPR data, which need to be filtered and analysed for quality assessment and usage. Before applying any processing algorithm, it is essential to edit the data. In fact, the rover collects LPR A-scans continuously, even when it stops to acquire other data. All such repeated redundant scans must be properly recognized and removed during a dedicated pre-processing (i.e. editing) phase.

The LPR dataset is then processed considering a basic and standard GPR processing flow integrated by surface information about the rover path, which was essential to perform topographic correction and identify artifacts on the LPR data. Furthermore, the rover path is not straight and it often has an almost duplicated route going back and forth along two similar trajectories. This reflects on the data with a peculiar symmetrical behavior with respect to the turnaround points. Identifying these artifacts is fundamental to avoid misinterpretation of the data¹².

A standard workflow from data download to quality control and data processing is an essential tool in order to make data analysis and interpretation reliable and objective. The ultimate goal is to improve the interpretation and comprehension of lunar subsurface structures, which in some cases were not previously imaged and properly considered. Signal data processing is in fact essential for all the GPR datasets to make possible a correct subsurface imaging and to estimate the electromagnetic physical parameters. In this light, the edited and ready-to-analyse datasets (Fig. 1) provided together with this article can represent a crucial starting point for future studies based on CE-4 data, but also on other integrated lunar analyses. All the data will be possibly integrated when further releases will be made available by the National Astronomical Observatory of the Chinese Academy of Sciences.

Methods

LPR data pre-processing and editing. Prior to the processing flow, that is usually performed on any GPR data acquired on the Earth, we considered the peculiar issues related to duplicated traces and data file stitching¹³. Considering the acquisition set up, the rover makes several stops to acquire other measurements during its movement, e.g. panoramic cam or visible near infrared spectroscopy, during which it does not interrupt the acquisition of LPR data. As a consequence, most of the raw data are redundant and must be removed. Since the accuracy of recorded coordinates is not high enough (see section Rover Coordinates), we have designed an algorithm capable of automatically recognizing and removing duplicated scans, minimizing the subjectivity of the procedure, saving time, and avoiding possible residual duplications (the complete code is freely available at https://github.com/Giacomo-Roncoroni/LPR_CE4/).

The proposed workflow summarized and described here is therefore implemented to reduce unwanted features, while retaining just the actual information contained into the dataset:

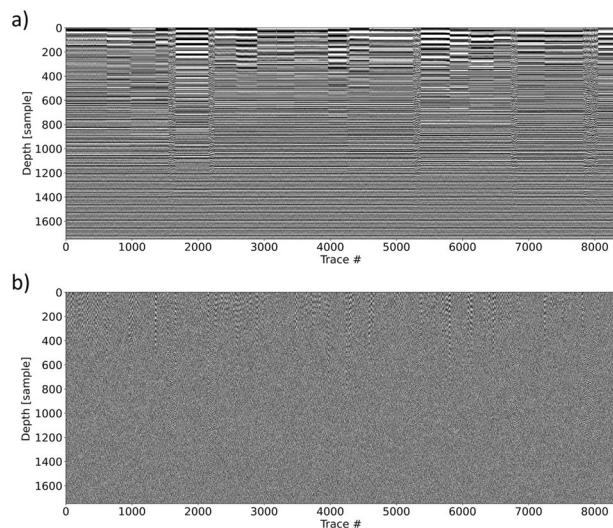


Fig. 2 SOL2 after de-wow (a) and Sobel filter (b).

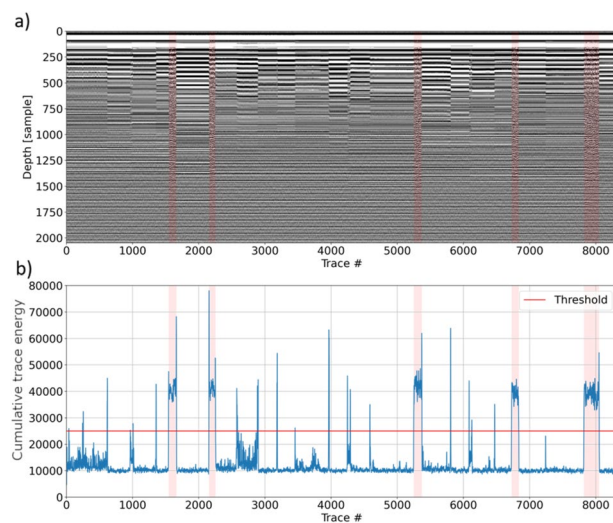


Fig. 3 Portion of raw data (a) and a corresponding energy plot (blue curve), set threshold (red line), (b). Selected scans related to the moving rover are marked in light red.

- Open separated PDS4 files selecting all LPR data and coordinates.
- Apply a de-wow, i.e., removing the first 300 samples of the dataset, due to the presence of clipped amplitudes (Fig. 2a).
- Apply a Sobel filter in x direction with a kernel size of 5, in order to suppress signals from the zones where the rover was not moving (Fig. 2b).
- Apply a median filter to reduce spikes and random noise in the dataset.
- Compute trace energy, i.e., sum the absolute values of the filtered traces along the time axis.
- Select just the energy values, within a set window (16 traces), that are over a threshold value (25000), kept constant for the whole dataset. These values were selected by a grid search on the parameters on the data; slightly different threshold values indeed produce almost identical outputs.

The whole procedure was first applied to identify the proper cutting of the limits/intervals, then we reapplied the workflow considering these intervals on the unprocessed data in order to not lose of information due to the Sobel filter (Fig. 3). Furthermore, the same windows and thresholds set above were applied also to data collected during the movement of the rover. The same procedure was applied to the entire dataset.

As mentioned above, data acquired in different lunar days are stored separately in different files (SOL) and need to be merged to get a manageable full dataset. From 634,419 A-scans stored in the original SOL files, after the duplication removal we obtained a 40,022 A-scans long LPR B-scan (i.e. profile). Figure 4 shows the

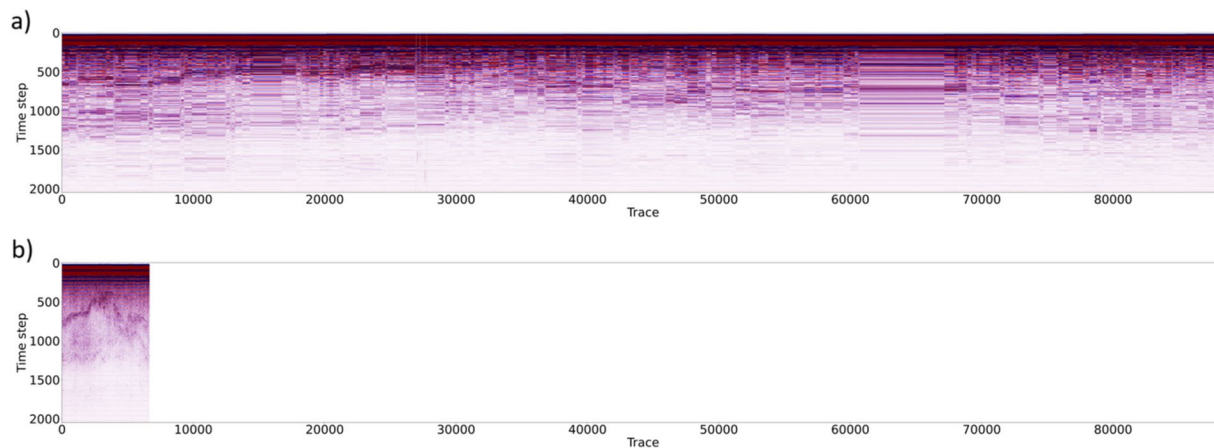


Fig. 4 Last 15% of the original dataset before (a) and after (b) redundant A-scans removal. Some subsurface reflectors are apparent in (b) while they are not recognizable in (a).

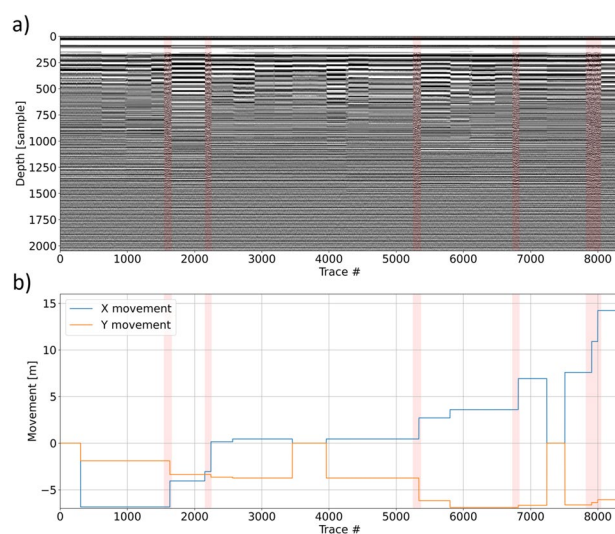


Fig. 5 LPR data (a) and the corresponding stored relative movement (extracted from the stored PDS4 coordinates) of the rover (b). Identified areas of actual movement (as in Fig. 3) are marked in light red.

reduction of redundant information on a portion of the dataset (from a to b) and the unprocessed data obtained after the duplicated scans removal (b). From Fig. 4b we can see the high quality of the data on which some subsurface structures are already apparent.

Rover coordinates. LPR data stored are not the only data affected by data redundancy and the other issues highlighted above: also acquisition coordinates are affected in the same way. If the stored coordinates were accurate enough, they could be used to select and retain only the scans associated to the actual rover movement, but this is not the case (Fig. 5). In fact, there are zones in which the coordinates change implying a rover movement which, however, did not take place considering that the A-scans recorded at these locations are indeed identical (e.g. near traces 300 or 7500).

Figure 6 compares the rover path extracted from the data filtered as described above and the one provided by Hoppe, 2022 (available at <http://lroc.sese.asu.edu/posts/1248>). It can be seen that the main mismatch occurs at the beginning and at the end (for the red line) of the rover path. The mean error is equal to 7.33 m with a standard deviation equal to 5.32 m.

Knowing the rover path details is essential to better discriminate evidence of actual subsurface structures on the data, avoiding interpreting signals which are just due to rover turnarounds and repeated paths. Information about data positioning allowed us to georeference the LPR data in the absolute location.

As the rover movements information in original PDS4 files are provided in meters, we decided to reproject the rover path on a metric reference system with an origin that corresponds to the CE-4 landing site, always assuming a constant A-scan distance for each selected portion of actual movement. As a result, we reprojected to our custom reference system also

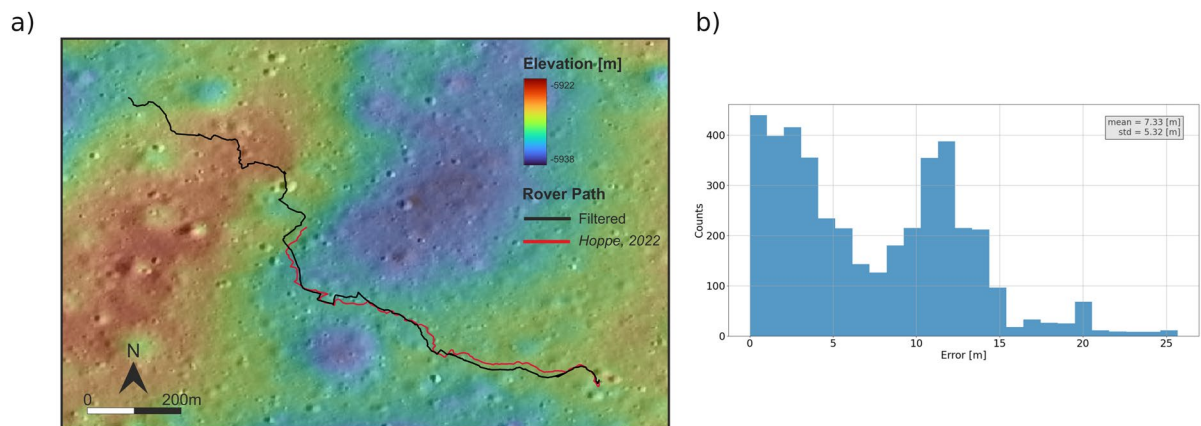


Fig. 6 Rover path extracted following our procedure (in black) and the one derived in Hoppe, 2022, (a) and histogram of the differences between the two estimated paths, (b).

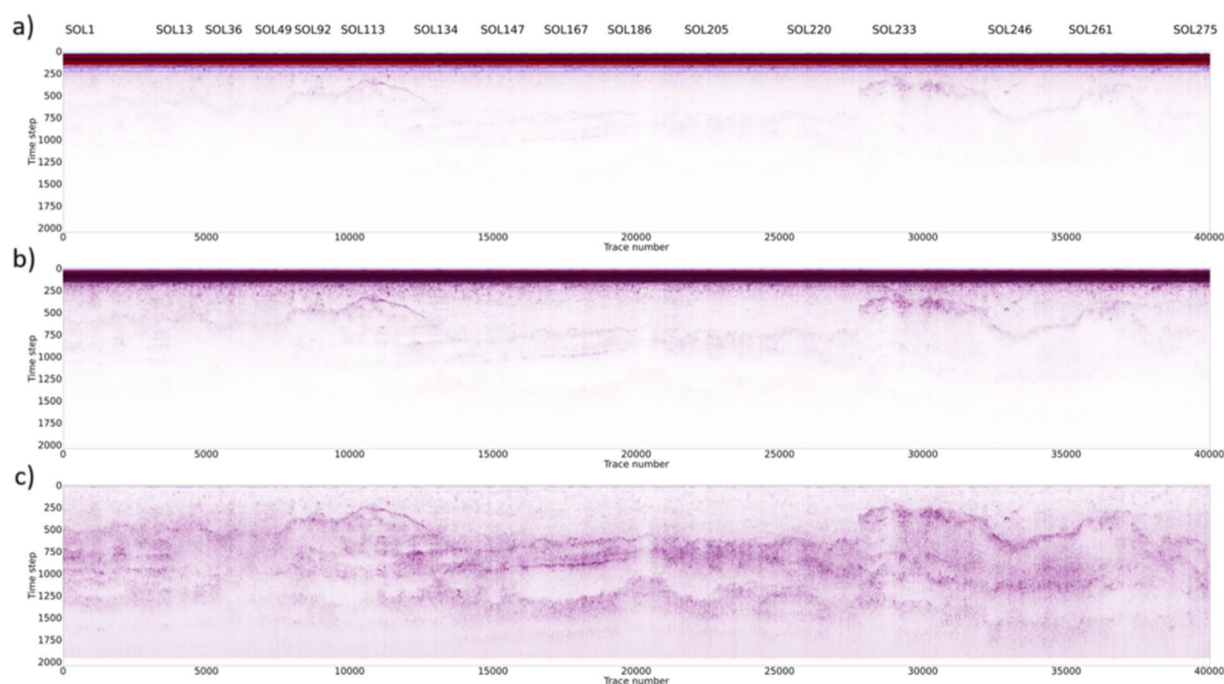


Fig. 7 Effects of the processing workflow applied on the whole dataset: raw data (a); data after the zero-time correction and bandpass filtering (b); data after horizontal high pass and gain in addition to the previous steps (c).

the orthophoto and the Digital Elevation Model (available at <https://quickmap.lroc.asu.edu/>). This latter step is mandatory for data integration and correlation of features evidenced on different datasets and imagery.

LPR data processing. Once the entire CE-4 dataset was edited (Fig. 7a), we applied a very conservative processing workflow to preserve the information related to amplitude and spectral content, both crucial for further data interpretation and analysis¹⁴.

The proposed processing workflow is performed in python and a step-by-step description and parametrization can be found at https://github.com/Giacomo-Roncoroni/LPR_CE4/tree/main/01_LPR_processing.

The proposed workflow¹⁴ is based on five main steps:

- Bandpass filter
- Zero-time correction (drift removal), Fig. 7b
- Horizontal High pass filter (background removal)
- Exponential amplitude compensation (gain), Fig. 7c
- Static (topographic) correction and depth conversion, Fig. 8

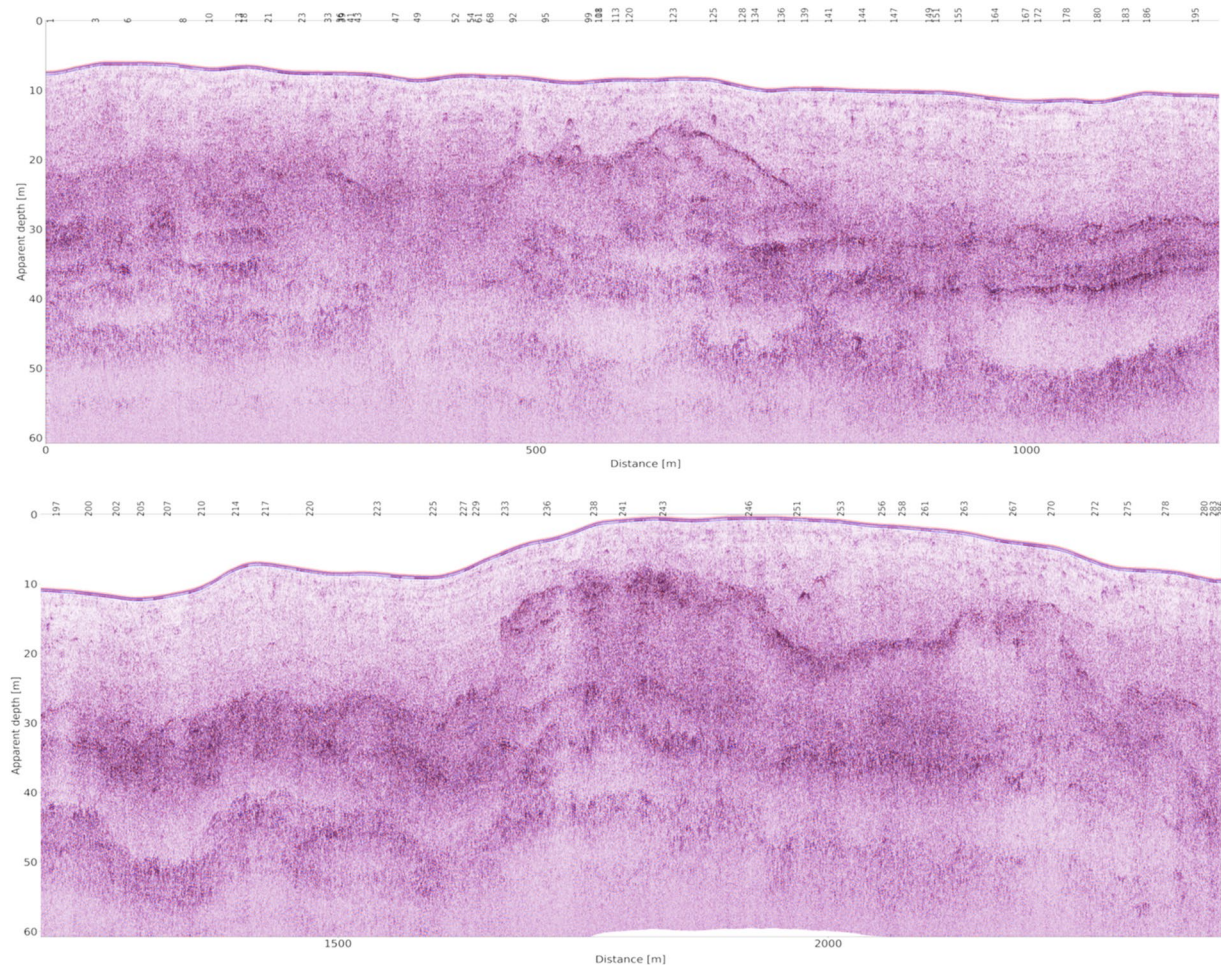


Fig. 8 Final processed CE-4 LPR dataset (split in two separate sections just for a better visualization) obtained after the application of the complete processing flow described in the text.

We applied a time to depth conversion with a constant velocity equal to 0.16 [m/ns], which is in good agreement with the most recent estimates^{15,16}. Other different non-constant estimates are available in literature, but their reliability and accuracy are still debated. The final processed data including static correction, i.e. correction of the position in the z direction applied, is shown in Fig. 8. Elevation data were derived by the Digital Elevation Model available on <https://quickmap.lroc.asu.edu/> considering A-scans with constant 0.036 m trace spacing¹⁷. The zero reference (datum) represents the maximum elevation of the rover along the considered path.

Data Records

The raw dataset is available in PDS4 format in Figshare¹⁸ and in SEG-Y format in Figshare¹⁹, maps and rover path are available in Figshare²⁰.

As shown in Fig. 1, the data resulting from our workflow are both edited and processed CE-4 LPR data, as well as their filtered spatial coordinates.

LPR data are stored as standard PDS4 and SEG-Y formats files with spatial information already saved in the file headers XPOSITION, YPOSITION and at bytes 73 and 77, respectively.

Specifically, the released PDS data are split in two files with extensions: 0.2BL for the text headers and 0.2B for the binary data files. The three datasets are:

- CE4_RAW_LPR_CH2_20190104_20230327_0000 → the edited data version, just filtered from the redundant repeated data.
- CE4_PROCESSED_LPR_CH2_20190104_20230327_0001 → the processed data version without the static (topographic) correction.
- CE4_PROCESSED_STATIC_LPR_CH2_20190104_20230327_0002 → the processed depth converted data version with static correction applied.

The three SEG-Y datasets are:

- 00_moon_final_raw → the edited data version, just filtered from the redundant repeated data.

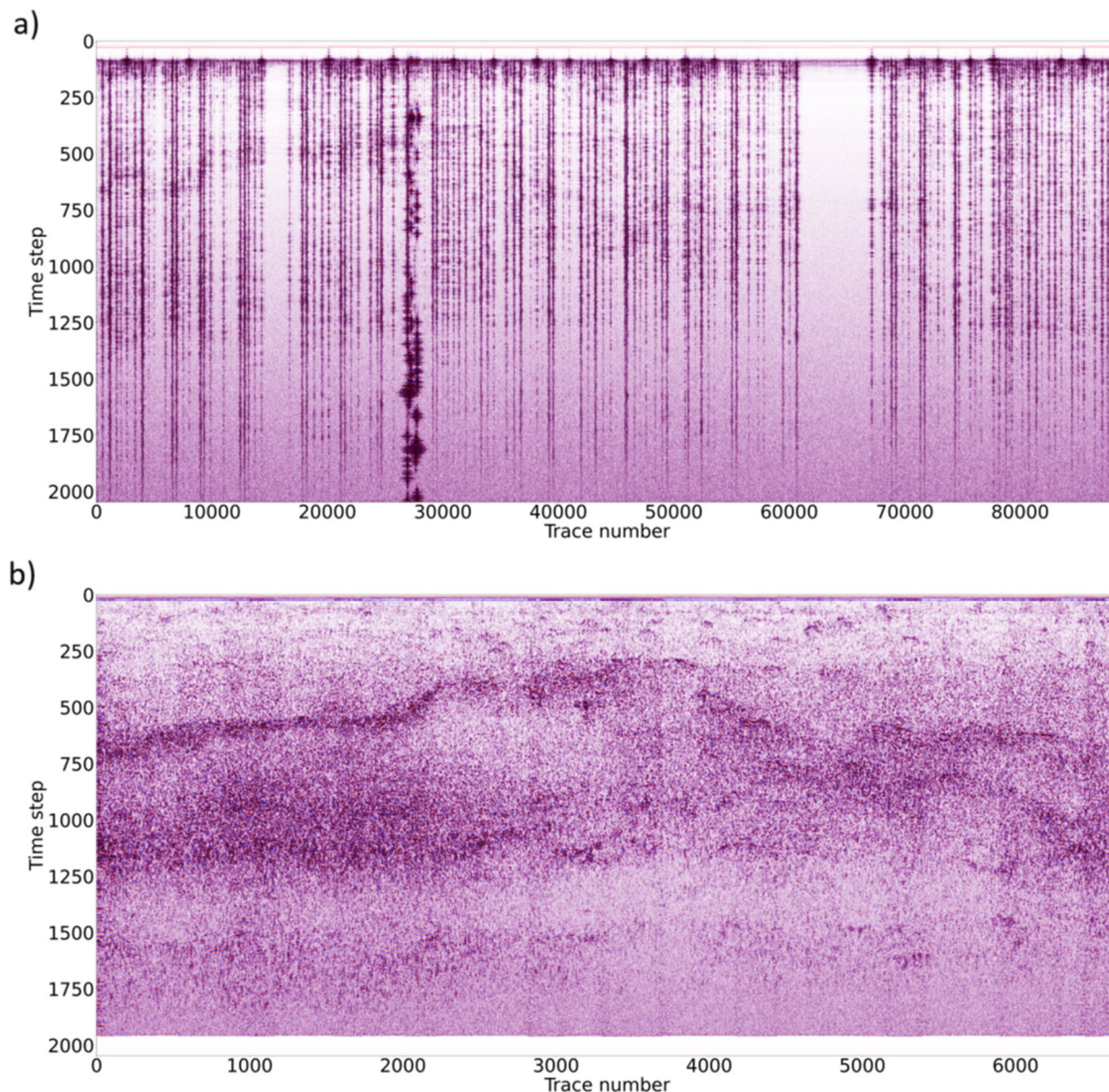


Fig. 9 Processing workflow applied to the complete original (redundant) dataset (a) and to the edited dataset after removal of all redundant records (b).

- 01_moon_final_proc → the processed data version without the static (topographic) correction.
- 02_moon_final_proc_static → the processed depth converted data version with static correction applied.

Coordinates files are store as text files (.txt) and are relative to the landing site (having 0, 0 coordinated): positive y are northwards and positive x are eastwards.

We also include the orthophoto and the DEM also centered in [0, 0] at the landing site.

Technical Validation

In order to prove the validity of the methodology, we applied the previously described processing methodology both on original and filtered data (Fig. 9). As we can see in Fig. 9a, it is impossible to interpret the original dataset due to data redundancy, while Fig. 9b shows filtered data in which several reflectors can be easily identified.

Moreover, in order to check the performances of the methodology, in Fig. 10 we highlight that the lateral continuity of the tilted reflector is guaranteed after the application of our methodology, even at the connection between originally separated data files, marked with vertical black lines in Fig. 10. In particular, we checked the signal phase behavior by calculating the cosine of the instantaneous phase (see e.g.²¹) which already demonstrated its capability to highlight signal phase discontinuities, even when GPR signals are characterized by similar amplitudes²².

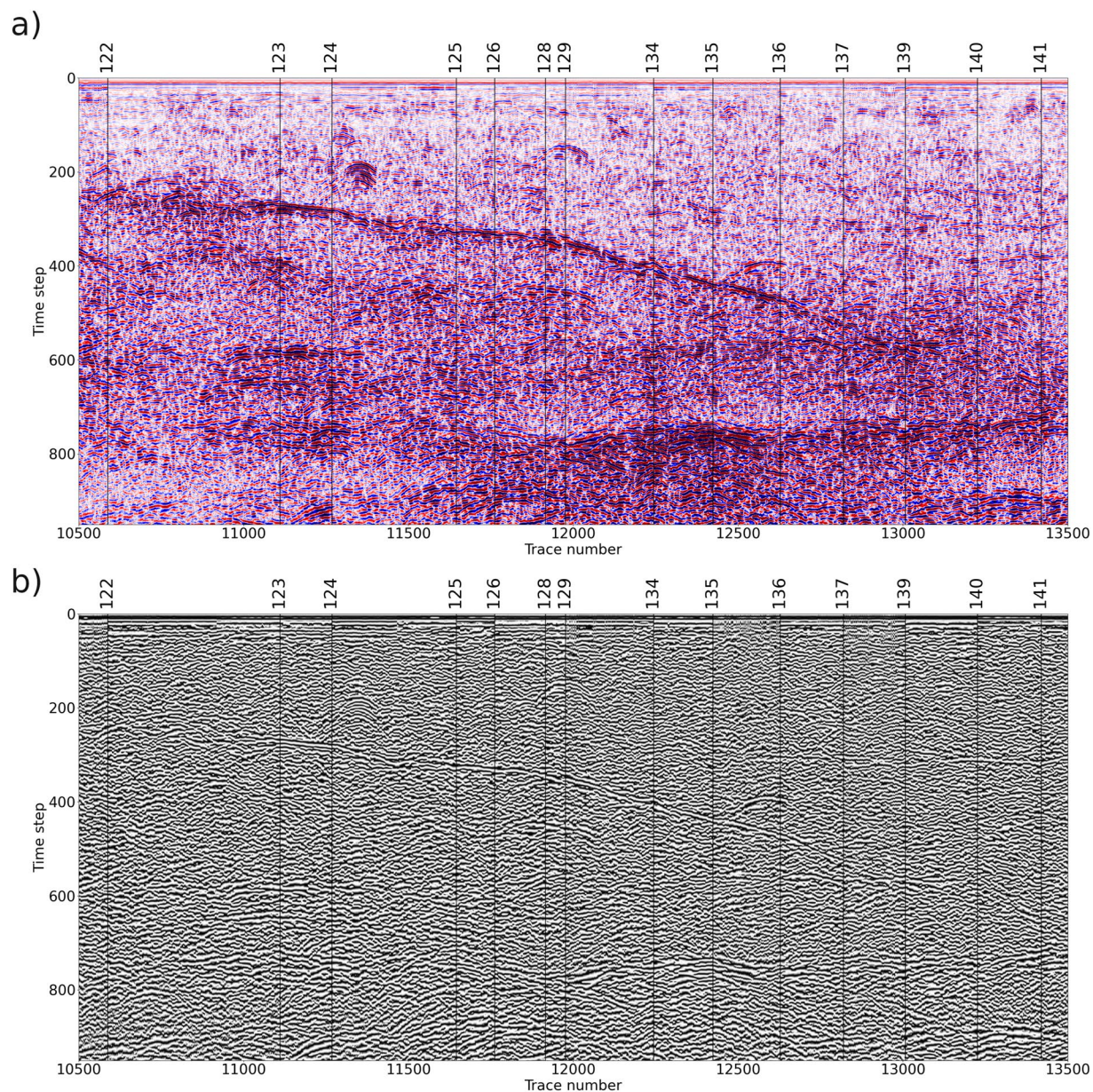


Fig. 10 Test on lateral continuity on an exemplary portion of the edited and processed dataset with superimposed the SOL numbers as for the original released data. **(a)** signal amplitude data; **(b)** cosine of instantaneous phase data.

Variable	Value	Units
Number of traces (A-scans) retained after the redundant traces removal	40022	[adimensional]
Number of time samples per trace	2048	[adimensional]
Nominal signal central frequency	500	[MHz]
Time sampling interval	0.3125	[ns]
Trace distance	0.036	[m]
EM velocity used for static correction and depth conversion	0.16	[m/ns]

Table 1. Summary of the main data parameters.

SEG-Y data provided in this paper are tested to properly work on different commercial and open-source programs namely: ProMAX (Halliburton), Petrel 17 (Schlumberger), Seisew 2.22 (Dalmorneftegeofizika Geophysical Company), Prism 2.70.04 (Radar Systems), Reflex 9.5.7 (Sandmaier). PDS4 data have been properly opened using PDS4_tools (see https://github.com/Giacomo-Roncoroni/LPR_CE4/tree/main/03_create_pds4).

Usage Notes

A summary of the main data parameters is presented in Table 1. This data descriptor was peer reviewed in 2023 based on the data available on the platform at the time.

Code availability

The codes for the described algorithm will be available in Figshare²³ and at https://github.com/Giacomo-Roncoroni/LPR_CE4.

Received: 26 September 2023; Accepted: 12 January 2024;

Published online: 24 January 2024

References

- Byrne, C. J. The South Pole-Aitken Basin and the South Polar Region. in *The Far Side of The Moon: A Photographic Guide* (ed. Byrne, C. J.) 60–93 (Springer New York, 2008).
- Dong, Z. *et al.* Properties of lunar regolith on the Moon's farside unveiled by Chang'E-4 Lunar Penetrating Radar. *J. Geophys. Res. Planets* **126** (2021).
- Li, C. *et al.* Pitfalls in GPR data interpretation: false reflectors detected in lunar radar cross sections by Chang'E-3. *IEEE Trans. Geosci. Remote Sens.* **56**, 1325–1335 (2018).
- Pettinelli, E., Lauro, S. E., Mattei, E., Cosciotti, B. & Soldovieri, F. Stratigraphy versus artefacts in the Chang'E-4 low-frequency radar. *Nat. Astron.* **5**, 890–893 (2021).
- Wu, W. *et al.* Lunar far side to be explored by Chang'E-4. *Nat. Geosci.* **12**, 222–223 (2019).
- Fang, G.-Y. *et al.* Lunar Penetrating Radar onboard the Chang'E-3 mission. *Res. Astron. Astrophys.* **14**, 1607–1622 (2014).
- Jia, Y. *et al.* The scientific objectives and payloads of Chang'E-4 mission. *Planet. Space Sci.* **162**, 207–215 (2018).
- Giannakis, I., Zhou, F., Warren, C. & Giannopoulos, A. Inferring the shallow layered structure at the Chang'E-4 landing site: a novel interpretation approach using Lunar Penetrating Radar. *Geophys. Res. Lett.* **48** (2021).
- Wang, R. *et al.* A novel approach for permittivity estimation of lunar regolith using the Lunar Penetrating Radar onboard Chang'E-4 rover. *Remote Sens.* **13** (2021).
- Chen, R. *et al.* Sub-surface stratification and dielectric permittivity distribution at the Chang'E-4 landing site revealed by the Lunar Penetrating Radar. *Astron. Astrophys.* **664** (2022).
- Barry, K. M., Cavers, D. A. & Kneale, C. W. Recommended standards for digital tape formats. *Geophysics* **40**, 344–352 (1975).
- Forte, E., Roncoroni, G. & Pipan, M. Are Lunar Penetrating Radar data so unusual? Some relevant issues about their processing and analysis. *Proceedings of the 12th International Workshop on Advanced Ground Penetrating Radar*, 12IWAGPR, 5th - 7th July 2023, Lisbon, Portugal, (2023).
- Lai, J. *et al.* A complex paleo-surface revealed by the Yutu-2 rover at the lunar farside. *Geophys. Res. Lett.* **48** (2021).
- Jol, H. M. *Ground Penetrating Radar: Theory and Applications* 4th edn (Elsevier, 2009).
- Feng, J., Siegler, Matthew A. & White, M.N. Dielectric properties and stratigraphy of regolith in the lunar South Pole-Aitken basin: observations from the Lunar Penetrating Radar. *Astron. Astrophys.* **661** (2022).
- Guo, D., Fa, W., Zeng, X., Du, J. & Liu, J. Geochemistry of the Von Kármán crater floor and thickness of the non-mare ejecta over the Chang'E-4 landing area. *Icarus* **359** (2021).
- Li, C. *et al.* The Moon's far side shallow subsurface structure unveiled by Chang'E-4 Lunar Penetrating Radar. *Sci. Adv.* **6** (2020).
- Roncoroni, G. PDS-4 file. *figshare. Dataset*. <https://doi.org/10.6084/m9.figshare.23723976.v1> (2024).
- Roncoroni, G. SEG-Y data. *figshare. Dataset*. <https://doi.org/10.6084/m9.figshare.23723922.v1> (2024).
- Roncoroni, G. CE4 maps. *figshare. Figure*. <https://doi.org/10.6084/m9.figshare.23723925.v1> (2024).
- Barnes, A. E. A tutorial on complex seismic trace analysis. *Geophysics* **72**, W33–W43 (2007).
- Zhao, W., Forte, E., Colucci, R. R. & Pipan, M. High-resolution glacier imaging and characterization by means of GPR attribute analysis. *Geophys. J. Int.* **206**, 1366–1374 (2016).
- Roncoroni, G. LPR_CE4 codes, *figshare. Software*. <https://doi.org/10.6084/m9.figshare.23798466.v1> (2024).

Acknowledgements

AC acknowledges Rita Levi Montalcini Fellowship by the Italian Ministry for University and Research (MUR). We thank the Chang'E-4 payload team for mission operations and China National Space Administration for providing the Chang'E-4 data that made this study possible. This work was supported by the National Natural Science Foundation of China (11773023, 11941001, U1631124) and the Civil Aerospace Pre-research Project (D020302). The Chang'E-4 data used in this work is processed and produced by Ground Research and Application System (GRAS) of China's Lunar and Planetary Exploration Program, it can be downloaded at <http://moon.bao.ac.cn/>.

Author contributions

Roncoroni G.: Code conceptualization, code writing, technical validation and manuscript draft. Forte E.: Technical validation, manuscript draft and review. Santin I.: QGIS data preparation and SEG-Y data validation. Černok A.: Manuscript review and maps validation. Rajšić A.: Manuscript review. Frigeri A.: Manuscript review and PDS4 validation. Pipan M.: Coordination and final manuscript review.

Competing interests

The authors declare no competing interests.

Additional information

Correspondence and requests for materials should be addressed to G.R.

Reprints and permissions information is available at www.nature.com/reprints.

Publisher's note Springer Nature remains neutral with regard to jurisdictional claims in published maps and institutional affiliations.



Open Access This article is licensed under a Creative Commons Attribution 4.0 International License, which permits use, sharing, adaptation, distribution and reproduction in any medium or format, as long as you give appropriate credit to the original author(s) and the source, provide a link to the Creative Commons licence, and indicate if changes were made. The images or other third party material in this article are included in the article's Creative Commons licence, unless indicated otherwise in a credit line to the material. If material is not included in the article's Creative Commons licence and your intended use is not permitted by statutory regulation or exceeds the permitted use, you will need to obtain permission directly from the copyright holder. To view a copy of this licence, visit <http://creativecommons.org/licenses/by/4.0/>.

© The Author(s) 2024